Out-of-time-order correlators of nonlocal block-spin and random observables in integrable and nonintegrable spin chains

Rohit Kumar Shukla,[1,*] Arul Lakshminarayan,[2,†] and Sunil Kumar Mishra[1,‡]
[1]*Department of Physics, Indian Institute of Technology (Banaras Hindu University), Varanasi 221005, India*
[2]*Department of Physics, Indian Institute of Technology Madras, Chennai 600036, India*

(Received 10 March 2022; accepted 1 June 2022; published 13 June 2022)

Out-of-time-order correlators (OTOC) in the Ising Floquet system, which can be both integrable and nonintegrable, are studied. Instead of localized spin observables, we study contiguous symmetric blocks of spins or random operators localized on these blocks as observables. We find only power-law growth of OTOC in both integrable and nonintegrable regimes. In the nonintegrable regime, beyond the scrambling time, there is an exponential saturation of the OTOC to values consistent with random matrix theory. This motivates the use of "prescrambled" random block operators as observables. A pure exponential saturation of OTOC in both integrable and nonintegrable system is observed, without a scrambling phase. Averaging over random observables from the Gaussian unitary ensemble, the OTOC is found to be exactly same as the operator entanglement entropy, whose exponential saturation has been observed in previous studies of such spin chains.

DOI: 10.1103/PhysRevB.105.224307

I. INTRODUCTION

Periodically driven Floquet systems have been extensively studied in the recent past in both classical and quantum system. A popular set of models are driven by fields applied in the form of kicks [1–4], as analytical forms of the time evolution operator are easy to find. One textbook example is the kicked-rotor model of a particle moving on a ring [5]. These models show interesting behavior, displaying transition from integrability to chaos, dynamical Anderson localization [5–7], and dynamical stabilization [8,9]. These systems are of interest in both classical and quantum systems. Such periodic forcing has been realized in experiments to study various phenomena [10–14].

In contrast to the kicked rotor, the Ising model with time-periodic transverse and longitudinal magnetic fields is an example of a many-body Floquet system of current interest [2,3,15,16]. Absence of a transverse component renders the system trivially integrable. Presence of both a longitudinal and transverse magnetic component makes this system nonintegrable. However, in the absence of longitudinal field, the system is rendered integrable as a system of noninteracting fermions. These systems have been studied using sudden quenches [17] and slow annealing [18]. In the quenched case, the system is out of equilibrium, leading to interesting dynamics of the observables, and has drawn considerable attention in the past decade with significant theoretical and experimental observations [19–21].

A typical way to distinguish among integrable, nonintegrable, and near-integrable regimes has been to use spectral properties and random matrix theory. This mostly leaves aside the question of dynamics. However, a quantity that has been extensively used recently to distinguish the chaotic and integrable dynamics is the out-of-time-order correlator (OTOC) [22–27]. In classical physics, one hallmark of chaos is that a small difference in the initial condition results in the exponential deviation of the trajectory, which is responsible for the so-called butterfly effect [28–30]. Classical Hamiltonian systems can have such pure deterministic chaos, which is used in the quantum domain for the study of quantum chaos [31,32]. It has been proposed that quantum chaos be characterized by the growth rate of OTOC [33], an exponential growth defining a quantum Lyapunov exponent.

Spin systems have been a playground for understanding many-body physics in general and growth of OTOCs in particular [24,26,34–43]. Growth of OTOC is discussed in systems such as Luttinger liquids [42], XY model [41], Sachdev-Ye-Kitaev (SYK) model [44], Heisenberg XXZ model, and Aubry-André-Harper model [26,43]. Lin and Motrunich [34] calculated OTOC for single-spin observables in the integrable transverse-field Ising model, and observed power-law growth, with the power varying with the separation between the localized spins.

Fortes *et al.* [38] studied OTOCs in the time-independent Ising model with tilted magnetic fields, perturbed XXZ model, and Heisenberg spin model with random magnetic fields. In all these models with single-spin observables, only power-law growth has been reported despite the presence of quantum chaos. OTOCs in integrable and nonintegrable Floquet Ising models were studied by Kukuljan *et al.* [37] using extensive observables. In the one-dimension case, the growth of OTOC density was still found to be linear in time.

The cases where exponential growth has been definitely reported involve semiclassical models such as the quantum kicked rotor [25], coupled kicked rotors [14,45], the kicked

*rohitkrshukla.rs.phy17@itbhu.ac.in
†arul@physics.iitm.ac.in
‡sunilkm.app@iitbhu.ac.in

top, which may be considered to be a transverse-field kicked Ising model but with the interactions being all to all [46,47], the bakers map [48], and so on. Our motivation herein is to allow for a large Hilbert space for the observables, which are restricted to blocks of spins. We may consider the spin chain as a bipartite chaotic system each consisting of $N/2$ spins to explore the possibility of exponential growth. We will see that such spin-1/2 nonintegrable models, even for block operators have only power-law OTOC growth, implying that their quantum Lyapunov exponents are 0.

In nonintegrable systems including spin chains such as studied here the long time saturation value of the OTOC is consistent with an estimate from random matrix theory. The approach of the OTOC to the saturation value was found to be at an exponential rate in weakly interacting bipartite chaotic system [45]. Exponential approach to saturation was also found in a semiclassical theory of OTOC [49]. We find such an exponential approach to the random matrix value in spin chains with block observables for the nonintegrable cases.

To understand the exponential approach, we consider the case when the block operators are random. Averaging over random unitary operators in bipartite system, the OTOC has been shown to be exactly the operator entanglement of the propagator [50]. We show this is also the case with random Hermitian observables, drawn from the Gaussian unitary ensemble (GUE).

Thus the exponential saturation of the OTOC is qualitatively consistent with the behavior previously observed for the operator entanglement growth of the propagator [51].

According to the BGS conjecture [52], the spectral properties of the quantum analog of a chaotic classical system will follow Wigner-Dyson statistics unlike the quantum analog of a integrable classical system following Poisson distribution. Thus, the spectral statistics of spacing between the consecutive energy levels of a quantum system works as a tool to differentiate a chaotic system from an integrable one [39,51,53–57].

This paper is organized as follows. In Sec. II A, we will discuss the Floquet map with and without longitudinal fields. In Sec. II B, we will define the OTOC for the block spin operators. In Sec. II C, we will discuss the relation of OTOC with operator entanglement entropy (OPEE). In the Sec. II D, we will elaborate the nearest-neighbor spacing distribution (NNSD) and its behavior in the integrable and nonintegrable cases. We will elaborate the behavior of OTOC and NNSD in Sec. III, for the constant-field Flqouet system, and in Sec. IV, for a special case of constant field Flquet system. Finally, in Sec. V, we will conclude the results.

II. SPIN MODEL AND BACKGROUND

A. Spin model

Consider a periodically driven Ising spin system with the Hamiltonian

$$\hat{H}(t) = J_x\hat{H}_{xx} + h_x\hat{H}_x + h_z\sum_{n=-\infty}^{\infty}\delta\Big(n-\frac{t}{\tau}\Big)\hat{H}_z. \qquad (1)$$

Here $\hat{H}_{xx} = \sum_{l=1}^{N-1}\hat{\sigma}_l^x\hat{\sigma}_{i+1}^x$ is the nearest-neighbor Ising interaction term, $\hat{H}_x = \sum_{l=1}^{N}\hat{\sigma}_l^x$ and $\hat{H}_z = \sum_{l=1}^{N}\hat{\sigma}_l^z$. The interaction strength is J_x, the continuous and constant longitudinal magnetic field in the x direction is given by h_x, and the transverse magnetic field in the z direction, which is applied in the form of δ pulses at regular interval τ, is h_z.

The Floquet operator is the propagator connecting states across one time period τ. Denoting this as $\hat{\mathcal{U}}_x$, we have (with $\hbar = 1$)

$$\hat{\mathcal{U}}_x = \exp[-i\tau(J_x\hat{H}_{xx} + h_x\hat{H}_x)]\exp(-i\tau h_z\hat{H}_z), \qquad (2)$$

which will be referred to as $\hat{\mathcal{U}}_x$ systems below, When the longitudinal field is absent, the model is solvable by the Jordan-Wigner transformation and renders the system as one of noninteracting fermions. In the presence of the longitudinal field, these fermions are interacting and there is evidence that there is a transition to quantum chaos [16,58–61]. The Floquet map of integrable model is a special case of Eq. (2) with $h_x = 0$ and will be referred to as the $\hat{\mathcal{U}}_0$ system below.

B. Out-of-time-order correlation and block operators

Dynamics of quantum systems lead to the spreading of initially localized operators under the unitary time evolution. Let the discrete time evolution of operator $\hat{W} \equiv \hat{W}(0)$ be $\hat{W}(n) = \hat{U}(n)^\dagger\hat{W}(0)\hat{U}(n)$, where $\hat{U}(n)$ is time-n propagator. For example, if the time evolution is governed by Eq. (2), $\hat{U}(n) = \hat{\mathcal{U}}_x^n$. If $\hat{V}$ and $\hat{W}$ are two Hermitian operators that are localized on different sets of spins (say A and B), we consider it as the out-of-time-order correlation (OTOC) [33,62–67],

$$C(n) = -\frac{1}{2\,d_A d_B}\mathrm{Tr}([\hat{W}(n),\hat{V}]^2), \qquad (3)$$

where d_A and d_B are dimensions of the subspaces, and $d_A = d_B = 2^{N/2}$ as we consider only the case of equal blocks. The OTOC $C(n)$ is clearly a measure of the noncommutativity of these two operators, via its norm.

This separates as $C(n) = C_2(n) - C_4(n)$, where $C_2(n)$ and $C_4(n)$ are two-point and four-point correlations respectively:

$$C_2(n) = \frac{1}{d_A d_B}\mathrm{Tr}(\hat{W}^2(n)\hat{V}^2), \qquad (4)$$

$$C_4(n) = \frac{1}{d_A d_B}\mathrm{Tr}(\hat{W}(n)\hat{V}\hat{W}(n)\hat{V}). \qquad (5)$$

These are infinite temperature quantities and involve the entire spectrum of 2^N states. We will use the trick of evaluating this by employing Haar random states of 2^N dimensions to evaluate expectation values, that is, $\mathrm{Tr}(\hat{A})/2^N \approx \langle\Psi_R|\hat{A}|\Psi_R\rangle$ where $|\Psi_R\rangle$ is such a state. Averages over a few random states are used.

Almost all studies of OTOC in such spin models thus far concentrate on operators that are localized on single spins; in contrast, we consider operators $\hat{V}$ and $\hat{W}$ initially isolated on the first and second block of spins, see Fig. 1, referred to here as spin-block operators (SBOs):

$$\hat{W} = \frac{2}{N}\sum_{l=1}^{\frac{N}{2}}\hat{\sigma}_l^x \quad \text{and} \quad \hat{V} = \frac{2}{N}\sum_{l=\frac{N}{2}+1}^{N}\hat{\sigma}_l^x. \qquad (6)$$

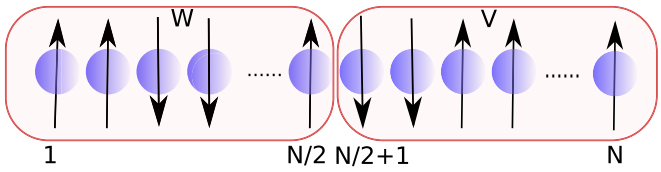

FIG. 1. Schematics of SBOs defined in Eq. (6). Even N is considered and halved into subsystems W and V.

Note that the behaviors of these OTOCs are genuinely different and do not follow from a knowledge of the single-site OTOCs involving correlations such as $\langle \hat{\sigma}^x_{l_1} \hat{\sigma}^x_{l_2}(n) \hat{\sigma}^x_{l_3} \hat{\sigma}^x_{l_4}(n) \rangle$ for general values of l_i. For $n > 0$, $\hat{W}(n)$ is no longer confined to the first $N/2$ spins, and the OTOC becomes nonzero.

C. Average and asymptotic OTOC values

As $\hat{V}$ and $\hat{W}$ are block-restricted sums of spin operators, $\hat{V} + \hat{W}$ is the total spin in the x direction and appears as a term in the Hamiltonian. Thus, these are special operators with dynamical significance, as would be natural to assume. In contrast, if they are random operators on the space of $N/2$ spins, the OTOC behaves quite differently until possibly the scrambling time. Beyond the scrambling time, we may expect that the local operators have largely become random if there is nonintegrability and quantum chaos. Thus, it is of interest to compare the behavior of random operator OTOC with nonrandom ones: to separate the effects of dynamics and scrambling. In a semiclassical model of weakly coupled chaotic systems, it was noted that the postscrambling time OTOC of nonrandom operators did behave as that of "prescrambled" random operators [45]. We find some similarties in the case of spin chains, but also interesting differences.

In the case of random operators for $\hat{V}$ and $\hat{W}$, ergodicity may be expected and hence an average over them is done. It has been observed [68] that if these operators are random unitaries chosen uniformly (Haar measure, circular unitary ensemble, CUE), the average OTOC is remarkably related to the operator entanglement. As we are using Hermitian operators, we average over random Hermitian ensembles for which we naturally choose the GUE, and the result is identical.

Let there be a bipartite space $\hat{\mathcal{H}}_A \otimes \hat{\mathcal{H}}_B$, such as the space of the first and second $N/2$ spins in the chain. The Schmidt decomposition of the unitary propagator on this bipartition is of the form

$$\hat{U}(n) = 2^{N/2} \sum_{i=1}^{2^N} \sqrt{\lambda_i(n)}\, \hat{A}_i(n) \otimes \hat{B}_i(n).$$

Here $\hat{A}_i(n)$ and $\hat{B}_i(n)$ are orthonormal operators on individual spaces $\hat{\mathcal{H}}_{A,B}$, satisfying $\mathrm{Tr}(\hat{A}_i(n)^\dagger \hat{A}_j(n)) = \mathrm{Tr}(\hat{B}_i(n)^\dagger \hat{B}_j(n)) = \delta_{ij}$. The numbers $\lambda_i(n) > 0$ and satisfy the condition $\sum_i \lambda_i(n) = 1$, which is a consequence of the unitarity of $\hat{U}(n)$.

Operator entanglement entropy (OPEE) is used for the measure of entanglement [51,68–70] and defined via the linear entropy as

$$E_l[\hat{U}(n)] = 1 - \sum_{i=1}^{2^N} \lambda_i^2(n). \tag{7}$$

This vanishes if and only if $\hat{U}(n)$ is of product form and is maximum when all $\lambda_i(n) = 2^{-N}$ and the OPEE is equal to $1 - 2^{-N}$.

Let an element of the GUE be $\hat{W} = (\hat{M} + \hat{M}^\dagger)/2$, where $\hat{M}$ is a d-dimensional matrix whose entries are such that its real and imaginary parts are zero centered, unit variance, independent normal random numbers, and the Ginibre ensemble. It is straightforward to see that $\overline{\hat{W}^2} = d\,\hat{I}_d$, where $\hat{I}_d$ is the d-dimensional identity matrix, and the overline indicates the GUE average. The average of $C_2(n)$ is then

$$\overline{C_2(n)}^{\hat{W},\hat{V}} = \frac{1}{d^2} \overline{\mathrm{Tr}(\hat{U}(n)^\dagger \hat{W}^2 \hat{U}(n) \hat{V}^2)}^{\hat{W},\hat{V}} = d^2, \tag{8}$$

where $\hat{V}$ is also a GUE realization independent of $\hat{W}$.

To evaluate the four-point function $C_4(n)$, we need to use the standard ploy of doubling the space: $\mathrm{Tr}(\hat{A}^2) = \mathrm{Tr}((\hat{A} \otimes \hat{A})\,\hat{S})$ where $\hat{S}$ swaps the original and ancilla spaces. With $\hat{A} = \hat{W}(n)\hat{V}$ the only relevant average needed is

$$\overline{\hat{W} \otimes \hat{W}}^{\hat{W}} = \hat{S}, \tag{9}$$

and it follows using identities known for the operator entanglement [50,68] that $\overline{C_4(n)}^{\hat{W},\hat{V}} = d^2[1 - E_l(\hat{U}(n))]$ and hence the OTOC averaged over the observables is

$$\overline{C(n)}^{\hat{W},\hat{V}} = d^2 E_l[\hat{U}(n)]. \tag{10}$$

Thus, the observable averaged OTOC is identical to the OPEE. Based on ergodicity, the case of a single random realization may then be expected to be represented by this average.

In the asymptotic limit of large times, if the dynamics is chaotic, we may expect that $\hat{U}(n)$ is a complex operator on the whole Hilbert space and treat it as being sampled according to the random CUE of size 2^N, while keeping $\hat{W}$ and $\hat{V}$ as fixed or nonrandom operators. The averaged quantities for traceless operators $\hat{V}$ and $\hat{W}$ are (see the Appendix for details)

$$\overline{C_2(n)}^{U} = \frac{1}{d^2} \mathrm{Tr}(\hat{W}^2)\mathrm{Tr}(\hat{V}^2), \tag{11a}$$

$$\overline{C_4(n)}^{U} = \frac{-1}{d^2(d^2-1)} \mathrm{Tr}(\hat{W}^2)\mathrm{Tr}(\hat{V}^2), \tag{11b}$$

$$\overline{C(n)}^{U} = \frac{1}{d^2-1} \mathrm{Tr}(\hat{W}^2)\mathrm{Tr}(\hat{V}^2). \tag{11c}$$

For the $\hat{W}$ and $\hat{V}$ in Eq. (6), the asymptotic value of the OTOC, ignoring the C_4 value, which is of lower order in the Hilbert space dimension, is this average and denoted below as

$$C(\infty) = 4/N^2. \tag{12}$$

For the GUE, random $\hat{V}$ and $\hat{W}$ used above $\overline{\mathrm{Tr}\hat{W}^2} = d^2$ and hence in this case $C(\infty) = d^2 = 2^{2N}$ for large d. We will always study scaled OTOC, dividing by the relevant $C(\infty)$, and thus for the random operator case, the averaged and scaled OTOC is exactly the OPEE $E_l[\hat{U}(n)]$.

D. Nearest-neighbor spacing distribution

Spectral statistics of the spacing between consecutive energy levels is used to differentiate the chaotic and integrable regimes. In order to calculate the NNSD, first we need to identify the symmetries of the Hamiltonian. Next, the Hamiltonian

is block diagonalized in the symmetry sectors. Our system with open boundary condition has a "bit-reversal" symmetry at all the Floquet periods. This bit-reversal symmetry is due to the fact that the field and interaction do not distinguish the spins by interchanging the spins at the sites i and $N-i+1$ for all $i = 1, \ldots, N$. Let us consider $\hat{B}$ a bit-reversal operator given by

$$\hat{B}|\mathrm{s}_1, \mathrm{s}_2, \ldots, \mathrm{s}_N\rangle = |\mathrm{s}_N, \ldots, \mathrm{s}_2, \mathrm{s}_1\rangle, \qquad [\hat{U}, \hat{B}] = 0, \tag{13}$$

where $|\mathrm{s}_i\rangle$ is any single-particle basis state in standard (s_z) basis. We divide the whole basis sets into two groups of basis states: One with the palindrome in which there is no change in the state after applying the operator $\hat{B}$, i.e., $\hat{B}|\mathrm{s}_1, \mathrm{s}_2, \ldots, \mathrm{s}_N\rangle = |\mathrm{s}_1, \mathrm{s}_2, \ldots, \mathrm{s}_N\rangle$. The other one with the nonpalindrome in which states get reflected after applying the operator $\hat{B}$, i.e., $\hat{B}|\mathrm{s}_1, \mathrm{s}_2, \ldots, \mathrm{s}_N\rangle = |\mathrm{s}_N, \ldots, \mathrm{s}_2, \mathrm{s}_1\rangle$. Since $\hat{B}^2 = 1$, the eigenvalues of $\hat{B}$ are ± 1. The eigenstates can be classified as odd or even state under bit reversal. All the palindromes define even states; however, all the nonpalindromes correspond to one even and one odd state. Sum and difference of the nonpalindrome and its reflection generate these even and odd states.

We study the shape of distribution by using the NNSD which may be used as an indicator of quantum chaos and nontrivial integrable models. In NNSD, strongly chaotic points are those where the unfolded level spacings are well described by the Wigner distribution [56,57,71], which is given as

$$P_W(s) = \frac{\pi s}{2} e^{-\pi s^2/4}, \tag{14}$$

where s is drawn from the ensemble of consecutive energy level separation. On the other hand, nontrivial integrable models are those where the unfolded NNSD follows Poisson statistics,

$$P_P(s) = e^{-s}. \tag{15}$$

III. CONSTANT FIELD FLOQUET SYSTEM

We analyze the OTOC given by Eq. (3) for the integrable $\hat{\mathcal{U}}_0$ and the nonintegrable $\hat{\mathcal{U}}_x$ systems defined in Sec. II A. The value of the magnetic fields is fixed at $h_x = 0$, $h_z = 4$ for the integrable case and $h_x = 4$, $h_z = 4$ for the nonintegrable case. The Floquet period τ acts as a parameter to drive the system into different dynamical regimes. In this paper, we will discuss the dynamic (prescrambling time) and saturation (postscrambling time) regions of OTOC, generated by spin-block operators defined in Eq. (6) as well as random operators referred to as RBO for "random block operators."

In the integrable case $\hat{\mathcal{U}}_0$ the dynamic region of the OTOC shows power-law growth, $C(n)/C(\infty) \sim n^b$, with the exponent being $b \approx 2$. This is shown in Fig. 2(a) for two values of the period, $\tau = \pi/18$ and $3\pi/18$. For period $0 < \tau < \pi/2$, the OTOC shows power-law growth with the same approximate quadratic growth, except at $\tau = \pi/4$, at which it vanishes. However, the OTOC does not saturate at any particular value beyond the scrambling time, as can be seen in inset of Fig. 2(a).

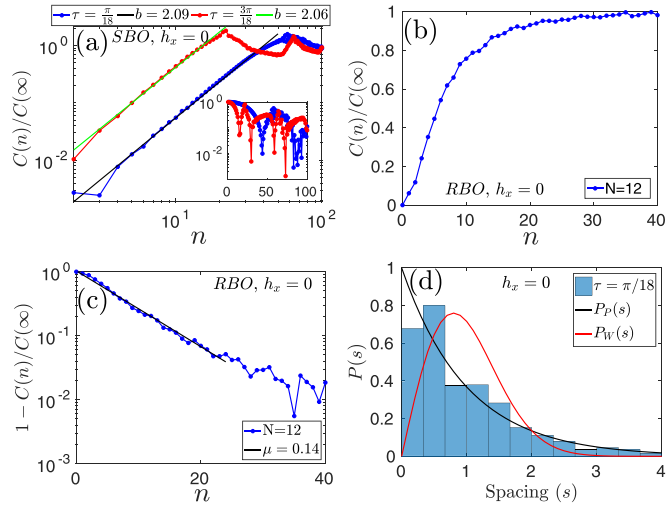

FIG. 2. Integrable $\hat{\mathcal{U}}_0$ system with parameters $\tau = \pi/18$, $J_x = 1$, $h_x = 0$, and $h_z = 4$. (a) $C(n)/C(\infty)$ generated by SBOs vs n for $N = 18$ and $\tau = \pi/18, 3\pi/18$ (log - log). Line with points represents data from the numerical calculation and solid line is the polynomial fitting. Inset shows $1 - C(n)/C(\infty)$ vs n (log -linear). (b) $C(n)/C(\infty)$ vs n for $N = 12$ and RBOs as observables. (c) $1 - C(n)/C(\infty)$ vs n for $N = 12$ and RBOs as observables. Line with points is data generated numerically and solid line is the exponential fitting. (d) NNSD for $N = 12$. In all the cases, open boundary condition is considered.

When we replace the spin operators with random block observables, the OTOC thermalizes quickly as compared to SBOs. This leads to disappearance of the power-law growth for $\tau = \pi/18$ [Fig. 2(b)] and is replaced by an exponential saturation $C(n)/C(\infty) \sim 1 - \exp(-\mu n)$, with the rate $\mu \approx 0.14$ [Fig. 2(c)]. The OTOC averaged over the random matrices $\hat{V}$ and $\hat{W}$ drawn from GUE for $\hat{\mathcal{U}}_0$ system is exactly same as OPEE $E_I[\hat{\mathcal{U}}_0]$, as established in Eq. (10).

Figure 2(d) shows that the NNSD of the integrable $\hat{\mathcal{U}}_0$ system at $\tau = \pi/18$ is of Poisson type rather than Wigner-Dyson type [34,38]. The system displays Poisson statistics at all the Floquet periods from $0 < \tau < \pi/2$ except at $\pi/4$. At $\tau = \pi/4$, as $h_z = 4$, the field term is effectively absent and $\hat{\mathcal{U}}_x = e^{-i\hat{H}_{xx}\frac{\pi}{4}}$, leading to vanishing OTOC, for the choice of spin observables.

OTOC in the nonintegrable $\hat{\mathcal{U}}_x$ system shows a power-law growth before the scrambling time, similar to that in the integrable $\hat{\mathcal{U}}_0$ case. However, in the nonintegrable case, the exponent of the power law is smaller as compared to the integrable case and the exponent increases with increasing τ. In order to extract the effects of nonitegrability, we focus on two τ values: $\tau = \pi/18$ and $3\pi/18$. At $\tau = \pi/18$ and $3\pi/18$, exponents of the power law are $b \approx 1.18$ and $b \approx 1.74$, respectively [Fig. 3(a)]. Hence, at $\tau = 3\pi/18$, the exponent is nearly quadratic in a power-law growth and independent of the system size, but the scrambling time of the OTOC depends on the system size: larger the size, longer is the scrambling time. Hence, the scrambling time of OTOC exhibits the finite-size effect as shown in Fig. 3(b). In a thermodynamic limit, we expect the scrambling time to occur after infinite number of kicks. OTOC approaches to saturation exponentially at any τ;

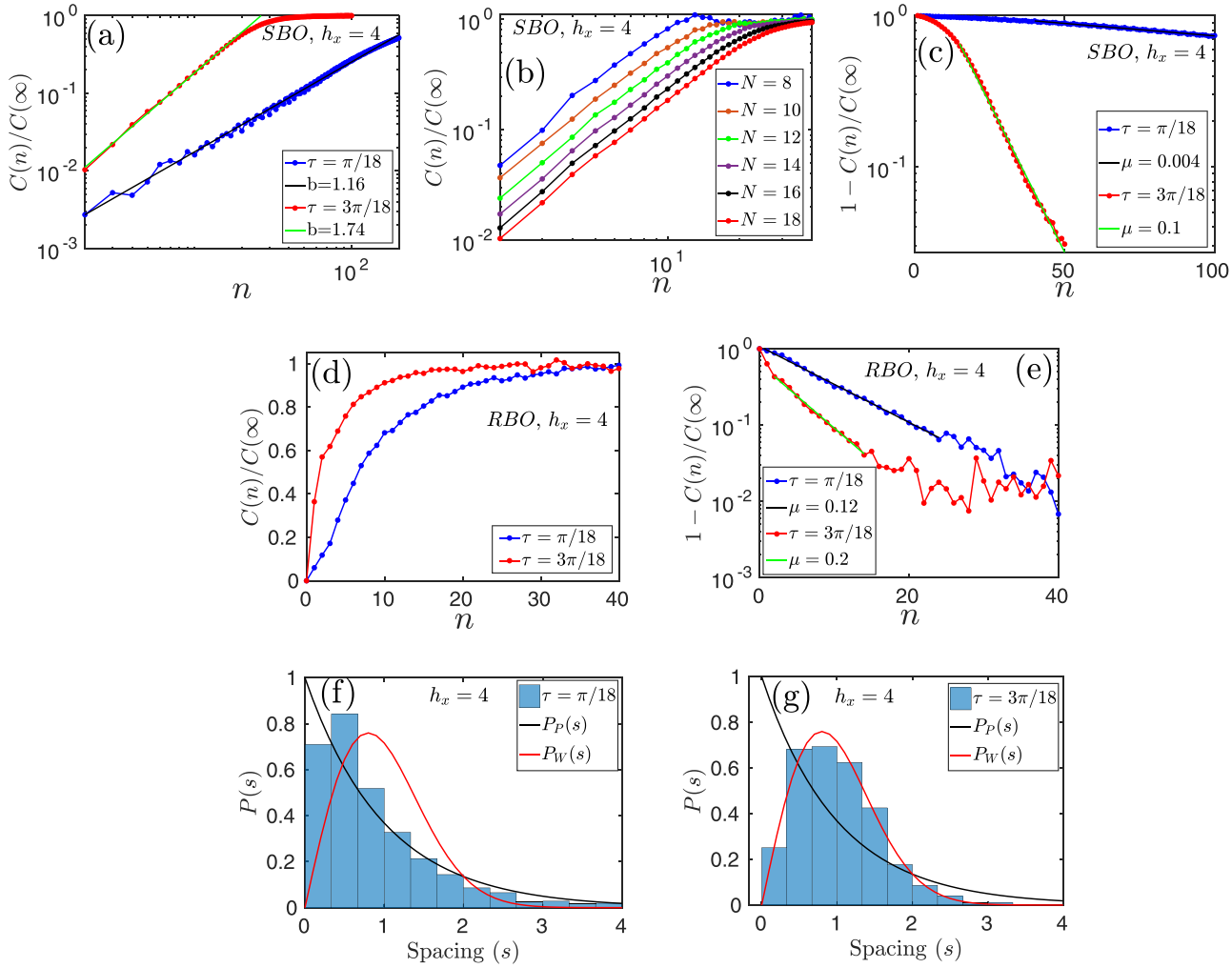

FIG. 3. Nonintegrable $\hat{\mathcal{U}}_x$ system with parameters $J_x = 1$, $h_x = 4$, $h_z = 4$, and $\tau = \pi/18, 3\pi/18$. (a) Illustrates the $C(n)/C(\infty)$ by using the SBOs vs n for $N = 18$ (log - log). Lines with points represent data from the numerical calculation and solid lines are the polynomial fitting with exponent $b \approx 1.18$ at $\tau = \pi/18$ and $b \approx 1.74$ at $\tau = 3\pi/18$. (b) $C(n)/C(\infty)$ by using the SBOs vs n at different N for $\tau = 3\pi/18$. (c) $1 - C(n)/C(\infty)$ vs n (log -linear). Lines with points are data generated numerically and solid lines are the exponential fitting. (d) Illustrates the OTOCs of RBOs vs n for $N = 12$. (e) $1 - C(n)/C(\infty)$ vs n (log -linear). Lines with points are data generated numerically and solid lines are the exponential fitting. NNSD of the $\hat{\mathcal{U}}_x$ system at (f) $\tau = \pi/18$ and (g) $\tau = 3\pi/18$ with $N = 12$. In all the cases, open boundary chain is considered.

however, the rate of saturation increases with increasing τ [see Fig. 3(c)].

Now, if we replace the localized spin observables $\hat{V}$ and $\hat{W}$ to prescrambled random block observables, the growth of OTOC does not show Lyapunov or power-law type at any τ [Fig. 3(d)]. It is exactly same as OPEE $E_l[\hat{\mathcal{U}}_x]$, as given by Eq. (10). OTOC saturates exponentially and the rate μ is ≈ 0.12 for $\tau = \pi/18$ and ≈ 0.20 for $3\pi/18$ as shown in Fig. 3(e). This is correlated with quantum chaos being prevalent at $\tau = 3\pi/18$, while $\tau = \pi/18$ seems to be near integrable.

This is consistent with the fact that NNSD of the nonintegrable Floquet system displays nearly Poissonian distribution at $\pi/18$ and Wigner-Dyson distribution at Floquet period $3\pi/18$ and moves toward Poisson distribution as the Floquet periods increases further from $3\pi/18$ to $\pi/4$. Therefore, we find $\tau = 3\pi/18$ as the most chaotic point in the Floquet system [Figs. 3(f) and 3(g)] in terms of NNSD.

The Floquet Ising model is special at $J_x\tau = \pi/4$, which was reported in different contexts earlier. With the choice of appropriate magnetic fields, such systems can show exact ballistic growth of block entanglement, revivals, and so on [2,4,51]. We will study a nontrivial example of this in the next section, in the context of OTOCs.

IV. SPECIAL CASE: $h_z = 1, h_x = 0, 1, \tau = \pi/4$

In the Ising Floquet system, there is a peculiar set of parameters, namely when $\tau = \pi/4$ for both the integrable $\hat{\mathcal{U}}_0$ case with $(h_x = 0, h_z = 1)$ and nonintegrable case $\hat{\mathcal{U}}_x$ with $(h_x = 1,\ h_z = 1)$. At this particular set of parameters, OTOC shows periodic oscillation in both integrable and nonintegrable systems. In the integrable case, OTOC oscillates with a time period equal to $2N$.

It attains a maximum value at $n = (2m - 1)N$ and goes to zero at $n = 2mN$, where $m \in \mathbb{Z}^+$ [Fig. 4(a)]. The maximum

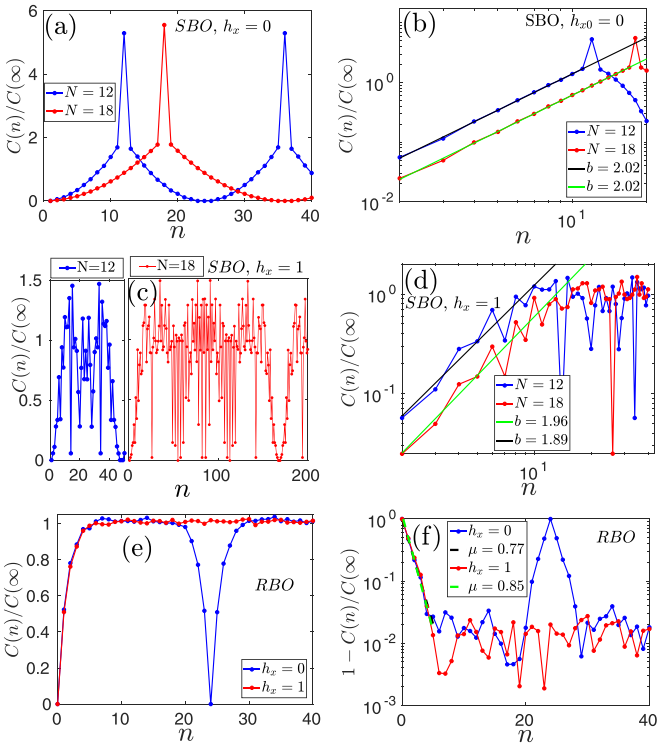

FIG. 4. (a) $C(n)/C(\infty)$ of SBOs vs n in the $\hat{\mathcal{U}}_0$ system for $N = 18$. (b) log - log behavior of (a) in which lines with points represent data from the numerical calculation and solid lines are the polynomial fitting. (c) $C(n)/C(\infty)$ of SBOs with n in the $\hat{\mathcal{U}}_x$ system for $N = 18$. (d) log - log behavior of (c) in which lines with points represent data from the numerical calculation and solid lines are the polynomial fitting. (e) $C(n)/C(\infty)$ of RBOs vs n in the $\hat{\mathcal{U}}_0$ and $\hat{\mathcal{U}}_x$ system for $N = 12$. (f) $1 - C(n)/C(\infty)$ vs n for $N = 12$ (log -linear). Lines with points are data generated numerically and solid lines are the exponential fitting. Other parameters: $J_x = 1$, $h_x = 0/1$, $h_z = 1$, and $\tau = \pi/4$. In all the cases, open boundary chain is considered.

value obtained is several times the saturation value of the nonintegrable case, namely $C(\infty)$. OTOC shows quadratic growth ($\sim n^b$, $b \approx 2$) until $N - 1$ kicks and the exponent is independent of the system size [Fig. 4(b)].

It should be noted that both the entanglement entropy of quenches and entangling power of the integrable $\hat{\mathcal{U}}_0$ model with open boundary condition [4,51] is maximum at times where OTOC is maximum. This is consistent with the so-called OTOC-RE theorem at infinite temperature that related OTOC to the second Renyi entropy S_V^2 as $C(n) \sim 1 - e^{-S_V^2} = 1 - \mathrm{Tr}\rho_V^2$ [72,73], where $S_V^2 = -\ln \mathrm{Tr}_V(\rho_V^2)$ behaves like von Neumann entropy [73,74]. Here $\rho_V = \mathrm{Tr}_W[\rho]$ is the reduced density matrix for the partition scheme for the block operators defined in Fig. 1.

The exact vanishing of the OTOC at $n = 2mN$, $m \in \mathbb{Z}^+$, follows as it has been shown earlier that the quasienergies of the $\hat{\mathcal{U}}_0$ are in the multiples of $\pi/(2N)$ such that as $\hat{\mathcal{U}}_0^{2N} = I$ [2]; therefore, in this case $\hat{W}(n = 2mN) = \hat{W}$ and the commutator $[\hat{W}(n = 2mN), V]$ becomes zero.

Similar to the integrable case, the nonintegrable $\hat{\mathcal{U}}_x$ case also shows a periodic behavior but the periodicity has a nontrivial unknown dependence on the system size [Fig. 4(c)]. Again, the OTOC grows approximately quadratically ($b \approx 2$) and independent of the system size [Fig. 4(d)]. However, there are increasing fluctuations and the maximum value attained is only about 1.5 times the random matrix value of $C(\infty)$ and if there is any system size dependence, it is weak.

Taking $\hat{V}$ and $\hat{W}$, as random matrices drawn from GUE, the power-law growth of OTOC gives way to initial exponential saturation in both integrable $\hat{\mathcal{U}}_0$ and nonintegrable $\hat{\mathcal{U}}_x$ systems. The exponent is nearly the same in both the cases ($\mu \approx 0.77$ for $h_x = 0$) and ($\mu \approx 0.85$ for $h_x = 1$) as shown in Fig. 4(f). The saturation value, although transient in the integrable case, is to a good approximation the random CUE value $C(\infty)$. For the integrable $\hat{\mathcal{U}}_0$ case, the periodic oscillation with time period equal to $2N$ remains as this is a property of the propagator. The OTOCs averaged over the random matrices $\hat{V}$ and $\hat{W}$ for $\hat{\mathcal{U}}_0$ and $\hat{\mathcal{U}}_x$ systems are exactly same as OPEE $E_l[\hat{\mathcal{U}}_0]$ and $E_l[\hat{\mathcal{U}}_x]$, respectively [see Eq. (10)].

For this special set of parameters, the spectrum of the Floquet operators, both integrable $\hat{\mathcal{U}}_0$ and nonintegrable $\hat{\mathcal{U}}_x$, are highly degenerate and we could not conclude the nature of distribution from the shape of NNSD. We observe that a small shift in τ from $\pi/4$ lifts this degeneracy. Therefore, it is useful to explore the proximity of $\tau = \pi/4$ by defining a small parameter (let us say $\epsilon = \pi/50$) such that the natural behavior of NNSD and OTOC does not change by adding or subtracting ϵ to $\tau = \pi/4$. We explore not only NNSD but also OTOC at the proximity of $\tau = \pi/4$.

In the integrable $\hat{\mathcal{U}}_0$ system with $\tau = \pi/4 - \epsilon$, we see OTOC deviates from the periodic behavior at $\tau = \pi/4$. Though we still see maxima and minima of OTOC near $n = (2m - 1)N$ and $2mN$ for $m \in \mathbb{Z}^+$, respectively, we observe that smaller the ϵ, sharper the maxima (minima) approaching to $n = (2m - 1)N$ ($n = 2mN$) [Fig. 5(a)]. We again get a quadratic power-law growth ($b \approx 2$) at $\tau = \pi/4 - \epsilon$ and the exponent is independent of the system size [Fig. 5(b)]. NNSD corresponding to this case displays nearly Poisson statistics in the integrable $\hat{\mathcal{U}}_0$ system [Fig. 5(c)].

On the other hand, OTOC in the nonintegrable $\hat{\mathcal{U}}_x$ system at $\tau = \pi/4 - \epsilon$ show a different behavior than that at $\pi/4$. There is no degeneracy in the spectrum, and the NNSD shows Wigner-Dyson distribution [Fig. 6(e)]. The OTOC grows until scrambling time and then saturates to the random matrix value of $C(\infty)$ [Fig. 6(a)]. The exact periodicity displayed at $\tau = \pi/4$ is not stable to perturbations, although the growth of OTOC is again quadratic ($b \approx 2$) and independent of the system size as well, as shown in Fig. 6(b).

Replacing $\hat{V}$ and $\hat{W}$ by prescrambled RBOs, we get a similar behavior of OTOC as that at $\tau = \pi/4$, in the $\hat{\mathcal{U}}_x$ system. However, in the $\hat{\mathcal{U}}_0$ system, the OTOC does not vanish at $n = 2mN$. This is due to the parameter ϵ which, if tending toward zero, lead to coinciding $\tau = \pi/4 - \epsilon$ case with $\tau = \pi/4$. Ideally OTOC for RBOs should also vanish at $n = 2mN$ due to the same reason that $\hat{W}(n = 2mN) = \hat{W}$ but with $\tau = \pi/4 - \epsilon$, we skip the moment of vanishing OTOC at $2mN$ kicks and get a dip only [Fig. 6(c)]. Again, we can confirm that OTOC averaged over the prescrambled RBOs is exactly the same as OPEE, as given in Eq. (10).

Figure 6(d) displays the initial exponential saturation of OTOC with nearly equal exponent in both integrable $\hat{\mathcal{U}}_0$

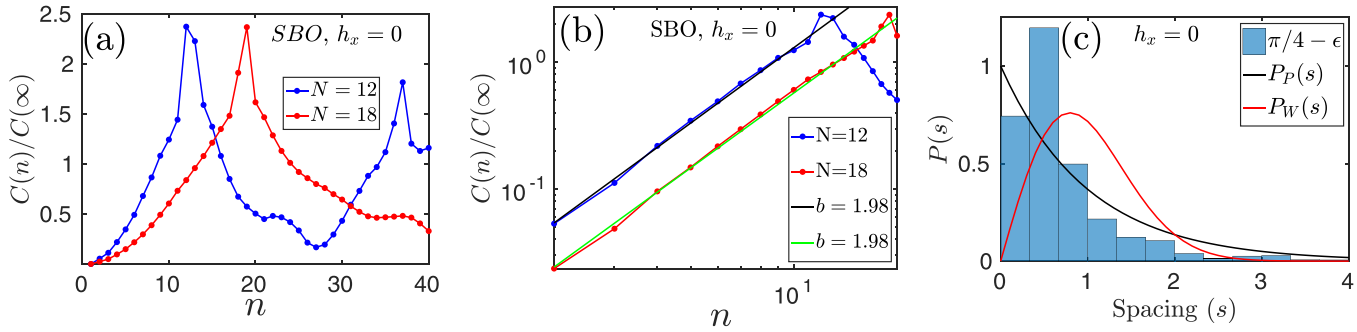

FIG. 5. Integrable $\hat{\mathcal{U}}_0$ system with parameters: $\tau = \pi/4 - \epsilon(= \pi/50)$, $J_x = 1$, $h_x = 0$, and $h_z = 1$. (a) $C(n)/C(\infty)$ of SBOs vs n in the $\hat{\mathcal{U}}_0$ system for $N = 18$. (b) log - log behavior of (a) in which lines with points represent data from the numerical calculation and solid lines are the polynomial fitting. (c) NNSD of the integrable $\hat{\mathcal{U}}_0$ system with $N = 12$.

and nonintegrable $\hat{\mathcal{U}}_x$ system ($\mu \approx 0.53$ for $\hat{\mathcal{U}}_0$ and $\mu \approx 0.56$ for $\hat{\mathcal{U}}_x$).

V. CONCLUSION

In this paper, we study the growth and saturation behavior of OTOC in both integrable $\hat{\mathcal{U}}_0$ and nonintegrable $\hat{\mathcal{U}}_x$ systems. The OTOC is calculated for observables as blocks of spins each consisting of $N/2$ spins defined as SBOs. Initially, we calculated OTOC by using the SBOs for various time periods and analyzed the early-time behavior and saturation behavior. Later, we used RBOs to learn about the saturation region of the system.

Growth of OTOC in both integrable $\hat{\mathcal{U}}_0$ and nonintegrable $\hat{\mathcal{U}}_x$ system shows power law for all Floquet periods in between $0 < \tau < \pi/2$ except $\pi/4$. This finding for nonlocal block spin as observables is consistent with single-site localized observables or total spin observables studied previously in the literature. At kick interval $\tau = \pi/4$, the field terms do not change the state; therefore, OTOC remains constant, even for the nonlocal block observables.

Later we take special parameters ($J_x = 1$, $h_z = 1$, $h_z = 0/1$, and $\tau = \pi/4$) and calculate the OTOC for the nonlocal SBOs. In the integrable system, we see a periodic trend and the period of oscillation is twice the system size. We also observe that the maxima and minima are those points where von Neumann entropy is also maxima and minima. In the nonintegrable $\hat{\mathcal{U}}_x$ case, periodic behavior does not show a trivial dependence on the system size. For $\tau = \pi/4$, OTOC shows a quadratic power-law growth in the integrable $\hat{\mathcal{U}}_0$

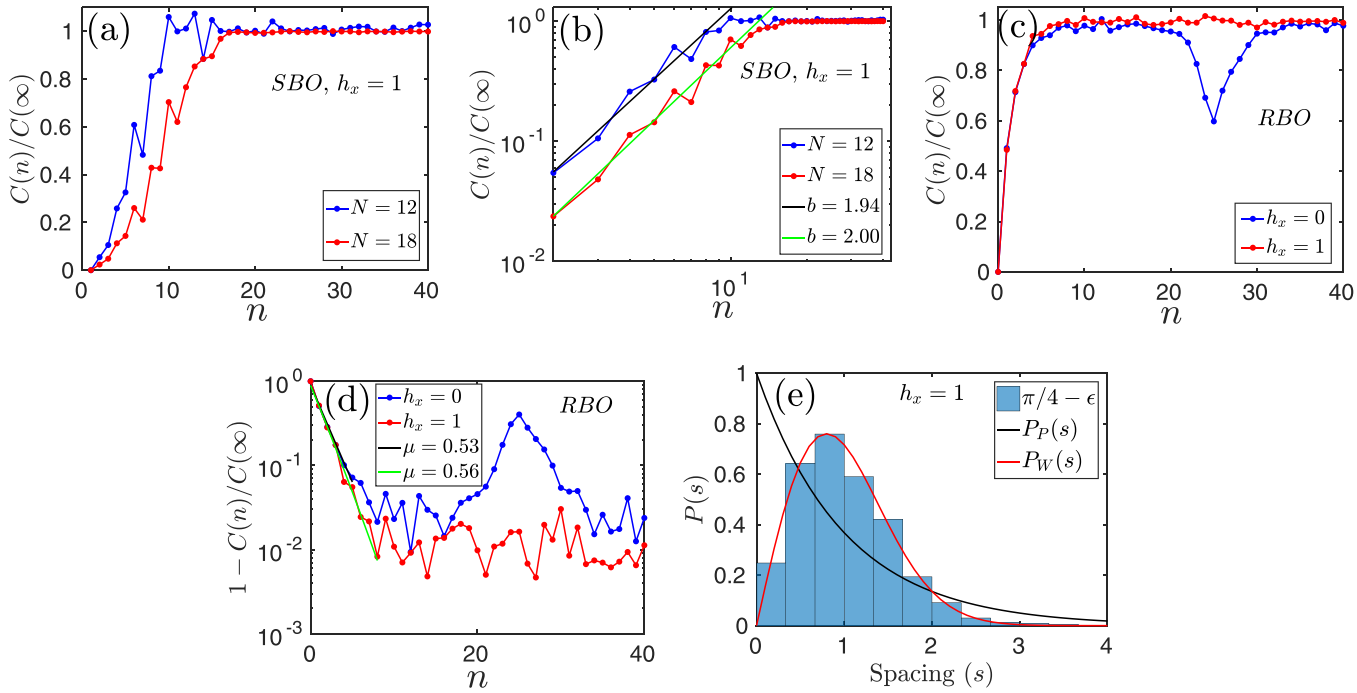

FIG. 6. (a) $C(n)/C(\infty)$ of SBOs vs n in the $\hat{\mathcal{U}}_x$ system for $N = 12$ and 18. (b) log - log behavior of (a) in which lines with points represent data from the numerical calculation and solid lines are the polynomial fitting. (c) $C(n)/C(\infty)$ of RBOs vs n in the $\hat{\mathcal{U}}_0$ and $\hat{\mathcal{U}}_x$ system for $N = 12$. (d) $1 - C(n)/C(\infty)$ vs n for $N = 12$ (log -linear). Lines with points are data generated numerically and solid lines are the exponential fitting. (d) NNSD of the $\hat{\mathcal{U}}_x$ system for $N = 12$. Other parameters: $J_x = 1$, $h_x = 0/1$, $h_z = 1$, and $\tau = \pi/4 - \epsilon(= \pi/50)$.

system until $n = N - 1$ kicks. We see a quadratic power law for the nonintegrable $\hat{\mathcal{U}}_x$ system as well. Large degeneracy at $\tau = \pi/4$ makes NNSD inconclusive whether it is Poisson or Wigner-Dyson type. In order to study the behavior approaching this Floquet period, we take a slightly lesser value of $\tau = \pi/4 - \pi/50$. At this τ, NNSD is Poisson type in the integrable $\hat{\mathcal{U}}_0$ system and Wigner-Dyson type in the nonintegrable $\hat{\mathcal{U}}_x$ system.

We also studied the postscrambling behavior of OTOC. In the nonintegrable $\hat{\mathcal{U}}_x$ system, OTOCs using SBOs show the exponential behavior that is consistent with random matrix theory. In the nonintegrable system, saturation behavior cannot be exactly defined by using the SBOs; therefore, we consider prescrambled RBOs and calculate OTOCs. We are getting the exponential saturation of the OTOC in all the cases which is consistent with the behavior previously observed for the operator entangling power.

In general, for a bipartite system, averaging over prescrambled random Hermitian observables, drawn from GUE, the OTOC is exactly same as the operator entanglement entropy.

APPENDIX: CALCULATION OF POST-SCRAMBLING OTOC USING RANDOM U

We calculate long time saturation values of OTOC for spin-block operators $\hat{V}$ and $\hat{W}$ by replacing the unitary operator $\hat{U}$ with random CUE of size 2^N and averaging over it. Two- and four-point correlation functions $C_2(n)$ and $C_4(n)$ are calculated as below.

1. Calculation of $C_2(n)$

Two-point correlation $[C_2(n)]$ averaged over random U drawn from CUE of size 2^N is given by

$$\overline{C_2(n)}^U = \frac{1}{d_A d_B}\overline{\mathrm{Tr}(\hat{W}(n)^2\hat{V}^2)}^U.$$

Time evolution of $\hat{W}$ is given by Heisenberg time evolution as $\hat{W}(n) = \hat{U}(n)^\dagger \hat{W}\hat{U}(n)$. Hence,

$$\begin{aligned}\overline{C_2(n)}^U &= \frac{1}{d_A d_B}\overline{\mathrm{Tr}(\hat{U}^\dagger\hat{W}^2\hat{U}\hat{V}^2)}^U \qquad \text{(A1)}\\ &= \frac{1}{d_A d_B}\sum_{j=1}^{d}\overline{\langle j|\hat{U}^\dagger\hat{W}^2\hat{U}\hat{V}^2)|j\rangle}^U,\\ &= \frac{1}{d_A d_B}\sum_{j,k,l,m}\overline{\langle j|\hat{U}^\dagger|k\rangle\langle k|\hat{W}^2|l\rangle\langle l|\hat{U}|m\rangle\langle m|\hat{V}^2|j\rangle}^U,\\ &= \frac{1}{d_A d_B}\sum_{j,k,l,m}\overline{\hat{U}^*_{kj}\hat{U}_{lm}}^U\hat{W}^2_{kl}\hat{V}^2_{mj}. \qquad \text{(A2)}\end{aligned}$$

Since $\overline{\hat{U}^*_{kj}\hat{U}_{lm}}^U = \sum_{j,k,l,m}\delta_{kl}\delta_{jm}|\hat{U}_{kj}|^2$ and $|\hat{U}_{kj}|^2 = \frac{1}{d}$,

$$\begin{aligned}\overline{C_2(n)}^U &= \frac{1}{d_A d_B}\frac{1}{d}\sum_{j,k,l,m}\delta_{kl}\delta_{jm}\hat{W}^2_{kl}\hat{V}^2_{mj},\\ &= \frac{1}{d_A d_B}\frac{1}{d}\sum_{k,j}\hat{W}^2_{kk}\hat{V}^2_{jj},\\ &= \frac{1}{d_A d_B}\frac{1}{d}\mathrm{Tr}(\hat{W}^2)\mathrm{Tr}(\hat{V}^2).\end{aligned}$$

Since $d_A d_B = 2^N$, $C_2(n)$ will be

$$C_2(n) = \frac{1}{2^{2N}}\hat{\mathrm{Tr}}(\hat{W}^2)\hat{\mathrm{Tr}}(\hat{V}^2). \qquad \text{(A3)}$$

Block observables are localized spin-block observables defined by Eq. (6). Then we calculate $\mathrm{Tr}(\hat{W}^2)$ will be

$$\mathrm{Tr}(\hat{W}^2) = \frac{4}{N^2}\mathrm{Tr}\left(\sum_{l=1}^{\frac{N}{2}}\left(\hat{\sigma}^x_l\right)^2 + \sum_{l\neq l'}\hat{\sigma}^x_l\hat{\sigma}^x_{l'}\right). \qquad \text{(A4)}$$

By using the properties of Pauli operator, the square of Pauli operators is equal to the identity matrix. Hence, the first term of Eq. (A4) will be equal to $\frac{2}{N}2^N$. The second term, $\sum_{l\neq l'}\hat{\sigma}^x_l\hat{\sigma}^x_{l'}$, is equal to zero because Pauli observable follows the anticommutation relation. Hence, $C_2(n)$ for the spin-block observables is

$$\overline{C_2(n)}^U = \frac{1}{2^{2N}}\frac{4}{N^2}2^{2N} = \frac{4}{N^2}. \qquad \text{(A5)}$$

2. Calculation of $C_4(n)$

The four-point correlator averaged over random U drawn from CUE of size 2^N is given by

$$\begin{aligned}\overline{C_4(n)}^U &= \frac{1}{d_A d_B}\overline{\mathrm{Tr}(\hat{W}(n)\hat{V}\hat{W}(n)\hat{V})}^U\\ &= \frac{1}{d_A d_B}\overline{\mathrm{Tr}(\hat{U}^\dagger\hat{W}\hat{U}\hat{V}\hat{U}^\dagger\hat{W}\hat{U}\hat{V})}^U\\ &= \frac{1}{d_A d_B}\sum_{i_1,i_2,\cdot,i_8}\overline{\langle i_1|\hat{U}^\dagger|i_2\rangle\langle i_2|\hat{W}|i_3\rangle\langle i_3|\hat{U}|i_4\rangle\langle i_4|\hat{V}|i_5\rangle\langle i_5|\hat{U}^\dagger|i_6\rangle\langle i_6|\hat{W}|i_7\rangle\langle i_7|\hat{U}|i_8\rangle\langle i_8|\hat{V}|i_1\rangle}^U\\ &= \frac{1}{d_A d_B}\sum_{i_1,i_2\cdot i_8}\overline{\hat{U}^*_{i_1,i_2}\hat{U}_{i_3,i_4}\hat{U}^*_{i_6,i_5}\hat{U}_{i_7,i_8}}^U\hat{W}_{i_2,i_3}\hat{V}_{i_4,i_5}\hat{W}_{i_6,i_7}\hat{V}_{i_8,i_1}\\ &= \frac{1}{d_A d_B}\sum_{i_1,i_2\cdot i_8}(\delta_{i_2,i_3}\delta_{i_1,i_4}\delta_{i_6,i_7}\delta_{i_5,i_8}|\hat{U}_{i_2,i_1}|^2|\hat{U}_{i_6,i_5}|^2\hat{W}_{i_2,i_3}\hat{V}_{i_4,i_5}\hat{W}_{i_6,i_7}\hat{V}_{i_8,i_1}\\ &\quad + \delta_{i_2,i_7}\delta_{i_1,i_8}\delta_{i_3,i_6}\delta_{i_4,i_5}|U_{i_2,i_1}|^2|\hat{U}_{i_3,i_4}|^2\hat{W}_{i_2,i_3}\hat{V}_{i_4,i_5}\hat{W}_{i_6,i_7}\hat{V}_{i_8,i_1})\end{aligned}$$

$$
\begin{aligned}
&- \frac{1}{d_A d_B} \sum_{i_1,i_2\cdot i_8} (\delta_{i_2,i_3}\delta_{i_1,i_4}\delta_{i_6,i_7}\delta_{i_5,i_8}\hat{U}^*_{i_2,i_1}\hat{U}_{i_2,i_4}\hat{U}^*_{i_6,i_5}\hat{U}_{i_6,i_8}\hat{W}_{i_2,i_3}\hat{V}_{i_4,i_5}\hat{W}_{i_6,i_7}\hat{V}_{i_8,i_1} \\
&+ \delta_{i_2,i_7}\delta_{i_1,i_8}\delta_{i_3,i_6}\delta_{i_4,i_5}U^*_{i_2,i_1}\hat{U}_{i_6,i_5}\hat{U}^*_{i_2,i_1}\hat{U}_{i_6,i_5}\hat{W}_{i_2,i_3}\hat{V}_{i_4,i_5}\hat{W}_{i_6,i_7}\hat{V}_{i_8,i_1}) \\
&= \frac{1}{d_A d_B}\frac{1}{d^2-1}\sum_{i_1,i_2\cdot i_8}(\delta_{i_2,i_3}\delta_{i_1,i_4}\delta_{i_6,i_7}\delta_{i_5,i_8}\hat{W}_{i_2,i_3}\hat{V}_{i_4,i_5}\hat{W}_{i_6,i_7}\hat{V}_{i_8,i_1} + \delta_{i_2,i_7}\delta_{i_1,i_8}\delta_{i_3,i_6}\delta_{i_4,i_5}\hat{W}_{i_2,i_3}\hat{V}_{i_4,i_5}\hat{W}_{i_6,i_7}\hat{V}_{i_8,i_1}) \\
&- \frac{1}{d_A d_B}\frac{1}{d(d^2-1)}\sum_{i_1,i_2\cdot i_8}(\delta_{i_2,i_3}\delta_{i_1,i_4}\delta_{i_6,i_7}\delta_{i_5,i_8}\hat{W}_{i_2,i_3}\hat{V}_{i_4,i_5}\hat{W}_{i_6,i_7}\hat{V}_{i_8,i_1} + \delta_{i_2,i_7}\delta_{i_1,i_8}\delta_{i_3,i_6}\delta_{i_4,i_5}\hat{W}_{i_2,i_3}\hat{V}_{i_4,i_5}\hat{W}_{i_6,i_7}\hat{V}_{i_8,i_1}) \\
&= \frac{1}{d_A d_B}\frac{1}{d^2-1}\sum_{i_1,i_2\cdot i_8}(\hat{W}_{i_1,i_2}\hat{V}_{i_1,i_5}\hat{W}_{i_6,i_6}\hat{V}_{i_5,i_1} + \hat{W}_{i_2,i_3}\hat{V}_{i_4,i_4}\hat{W}_{i_3,i_2}\hat{V}_{i_1,i_1}) \\
&- \frac{1}{d_A d_B}\frac{1}{d(d^2-1)}\sum_{i_1,i_2\cdot i_8}(\hat{W}_{i_2,i_2}\hat{V}_{i_4,i_4}\hat{W}_{i_6,i_6}\hat{V}_{i_8,i_8} + \hat{W}_{i_2,i_3}\hat{V}_{i_4,i_5}\hat{W}_{i_6,i_7}\hat{V}_{i_8,i_1}) \\
&= \frac{1}{d_A d_B}\frac{1}{d^2-1}((\mathrm{Tr}\hat{W})^2(\mathrm{Tr}\hat{V})^2 + (\mathrm{Tr}\hat{W}^2)(\mathrm{Tr}\hat{V})^2) \\
&- \frac{1}{d_A d_B}\frac{1}{d(d^2-1)}(\mathrm{Tr}(\hat{W}^2)\mathrm{Tr}(\hat{V}^2) + (\mathrm{Tr}\hat{W})^2(\mathrm{Tr}\hat{V})^2) + O\left(\frac{1}{d(d^2-1)}\right).
\end{aligned}
$$

Considering traceless observables such that $\mathrm{Tr}(\hat{W}) = 0$, $\mathrm{Tr}(\hat{V}) = 0$, and $d_A d_B = d$, we get

$$
\begin{aligned}
\overline{C_4(n)}^U &= -\frac{1}{d}\frac{1}{d(d^2-1)}(\mathrm{Tr}\hat{W}^2)(\mathrm{Tr}\hat{V}^2) \\
&= -\frac{1}{d^2(d^2-1)}(\mathrm{Tr}\hat{W}^2)(\mathrm{Tr}\hat{V}^2). \qquad \text{(A6)}
\end{aligned}
$$

For traceless observables $C_2(n)$ will be

$$
\overline{C_2(n)}^U = \frac{1}{d^2}\mathrm{Tr}(\hat{W}^2)\mathrm{Tr}(\hat{V}^2). \qquad \text{(A7)}
$$

Hence, OTOC for the traceless observables will be

$$
\begin{aligned}
\overline{C(n)}^U &= \overline{C_2(n)}^U - \overline{C_4(n)}^U \\
&= \frac{1}{d^2}(\mathrm{Tr}\hat{W}^2)(\mathrm{Tr}\hat{V}^2)\left(1 + \frac{1}{d^2-1}\right) \\
&= \frac{1}{d^2}(\mathrm{Tr}\hat{W})^2(\mathrm{Tr}\hat{V})^2\frac{d^2}{d^2-1} \\
&= \frac{1}{d^2-1}(\mathrm{Tr}\hat{W})^2(\mathrm{Tr}\hat{V})^2 \\
&= \frac{1}{2^{2N}-1} \\
&\approx \frac{1}{2^{2N}}. \qquad \text{(A8)}
\end{aligned}
$$

[1] L. D'Alessio and M. Rigol, Phys. Rev. X **4**, 041048 (2014).
[2] G. K. Naik, R. Singh, and S. K. Mishra, Phys. Rev. A **99**, 032321 (2019).
[3] R. K. Shukla, G. K. Naik, and S. K. Mishra, EPL **132**, 47003 (2021).
[4] S. K. Mishra, A. Lakshminarayan, and V. Subrahmanyam, Phys. Rev. A **91**, 022318 (2015).
[5] L. Reichl, *The Transition to Chaos: Conservative Classical Systems and Quantum Manifestations* (Springer Science & Business Media, Berlin, 2004).
[6] B. V. Chirikov, F. M. Izrailev, and D. L. Shepelyansky, Sov. Sci. Rev. C **2**, 209 (1981).
[7] S. Fishman, D. R. Grempel, and R. E. Prange, Phys. Rev. Lett. **49**, 509 (1982).
[8] P. L. Kapitza, *Collected Papers of PL Kapitza* (Pergamon, United Kingdom, 1965), Vol. 2, p. 714.
[9] H. Broer, I. Hoveijn, M. Van Noort, C. Simó, and G. Vegter, J. Dyn. Differ. Equations **16**, 897 (2004).
[10] K. Wintersperger, C. Braun, F. N. Ünal, A. Eckardt, M. D. Liberto, N. Goldman, I. Bloch, and M. Aidelsburger, Nat. Phys. **16**, 1058 (2020).
[11] S. Franca, F. Hassler, and I. C. Fulga, SciPost Phys. Core **4**, 007 (2021).
[12] J. Zhang, P. W. Hess, A. Kyprianidis, P. Becker, A. Lee, J. Smith, G. Pagano, I.-D. Potirniche, A. C. Potter, A. Vishwanath *et al.*, Nature (London) **543**, 217 (2017).
[13] S. Choi, J. Choi, R. Landig, G. Kucsko, H. Zhou, J. Isoya, F. Jelezko, S. Onoda, H. Sumiya, V. Khemani *et al.*, Nature (London) **543**, 221 (2017).
[14] J. B. K. M. S. Santhanam and S. Paul, Phys. Rep. **956**, 1 (2022).
[15] V. Gritsev and A. Polkovnikov, SciPost Phys. **2**, 021 (2017).
[16] A. Lakshminarayan and V. Subrahmanyam, Phys. Rev. A **71**, 062334 (2005).
[17] A. Polkovnikov, K. Sengupta, A. Silva, and M. Vengalattore, Rev. Mod. Phys. **83**, 863 (2011).
[18] G. E. Santoro, Science **295**, 2427 (2002).

[19] A. Russomanno, A. Silva, and G. E. Santoro, Phys. Rev. Lett. **109**, 257201 (2012).
[20] N. Russomanno, A. Silva, and G. E. Santoro, J. Stat. Mech.: Theory Exp. (2013) P09012.
[21] S. K. Mishra and A. Lakshminarayan, EPL **105**, 10002 (2014).
[22] I. García-Mata, M. Saraceno, R. A. Jalabert, A. J. Roncaglia, and D. A. Wisniacki, Phys. Rev. Lett. **121**, 210601 (2018).
[23] E. B. Rozenbaum, L. A. Bunimovich, and V. Galitski, Phys. Rev. Lett. **125**, 014101 (2020).
[24] H. Yan, J.-Z. Wang, and W.-G. Wang, Commun. Theor. Phys. **71**, 1359 (2019).
[25] E. B. Rozenbaum, S. Ganeshan, and V. Galitski, Phys. Rev. Lett. **118**, 086801 (2017).
[26] J. Lee, D. Kim, and D.-H. Kim, Phys. Rev. B **99**, 184202 (2019).
[27] E. B. Rozenbaum, S. Ganeshan, and V. Galitski, Phys. Rev. B **100**, 035112 (2019).
[28] Y. Gu and X.-L. Qi, J. High Energy Phys. 08 (2016) 129.
[29] T. Bilitewski, S. Bhattacharjee, and R. Moessner, Phys. Rev. Lett. **121**, 250602 (2018).
[30] A. Das, S. Chakrabarty, A. Dhar, A. Kundu, D. A. Huse, R. Moessner, S. S. Ray, and S. Bhattacharjee, Phys. Rev. Lett. **121**, 024101 (2018).
[31] M. C. Gutzwiller, *Chaos in Classical and Quantum Mechanics* (Springer Science & Business Media, Berlin, 2013), Vol. 1.
[32] F. Haake, *Quantum Coherence in Mesoscopic Systems* (Springer, Berlin, 1991), pp. 583–595.
[33] J. Maldacena, S. H. Shenker, and D. Stanford, J. High Energy Phys. 08 (2016) 106.
[34] C.-J. Lin and O. I. Motrunich, Phys. Rev. B **97**, 144304 (2018).
[35] S. Xu and B. Swingle, Nat. Phys. **16**, 199 (2020).
[36] S. Xu and B. Swingle, Phys. Rev. X **9**, 031048 (2019).
[37] I. Kukuljan, S. Grozdanov, and T. Prosen, Phys. Rev. B **96**, 060301(R) (2017).
[38] E. M. Fortes, I. García-Mata, R. A. Jalabert, and D. A. Wisniacki, Phys. Rev. E **100**, 042201 (2019).
[39] B. Craps, M. De Clerck, D. Janssens, V. Luyten, and C. Rabideau, Phys. Rev. B **101**, 174313 (2020).
[40] N. Roy and A. Sharma, J. Phys.: Condens. Matter **33**, 334001 (2021).
[41] J.-H. Bao and C.-Y. Zhang, Commun. Theor. Phys. **72**, 085103 (2020).
[42] B. Dóra and R. Moessner, Phys. Rev. Lett. **119**, 026802 (2017).
[43] J. Riddell and E. S. Sørensen, Phys. Rev. B **99**, 054205 (2019).
[44] W. Fu and S. Sachdev, Phys. Rev. B **94**, 035135 (2016).
[45] R. Prakash and A. Lakshminarayan, Phys. Rev. B **101**, 121108(R) (2020).
[46] C. Yin and A. Lucas, Phys. Rev. A **103**, 042414 (2021).
[47] P. Sreeram, V. Madhok, and A. Lakshminarayan, J. Phys. D **54**, 274004 (2021).
[48] A. Lakshminarayan, Phys. Rev. E **99**, 012201 (2019).
[49] J. Rammensee, J. D. Urbina, and K. Richter, Phys. Rev. Lett. **121**, 124101 (2018).
[50] N. Anand and P. Zanardi, arXiv:2111.07086.
[51] R. Pal and A. Lakshminarayan, Phys. Rev. B **98**, 174304 (2018).
[52] O. Bohigas, M. J. Giannoni, and C. Schmit, Phys. Rev. Lett. **52**, 1 (1984).
[53] J. Karthik, A. Sharma, and A. Lakshminarayan, Phys. Rev. A **75**, 022304 (2007).
[54] S. Ray, S. Sinha, and K. Sengupta, Phys. Rev. A **98**, 053631 (2018).
[55] X. Chen, T. Zhou, and C. Xu, J. Stat. Mech.: Theory Exp. (2018) 073101.
[56] M. L. Mehta, *Random Matrices*, 3rd ed. (Academic Press, Cambridge, MA, 2004).
[57] I. S. Averbukh and R. Arvieu, Phys. Rev. Lett. **87**, 163601 (2001).
[58] T. Prosen, Phys. D (Amsterdam, Neth.) **187**, 244 (2004).
[59] T. Prosen, Prog. Theor. Phys. Suppl. **139**, 191 (2000).
[60] T. Prosen, Phys. Rev. E **65**, 036208 (2002).
[61] D. V. Else, B. Bauer, and C. Nayak, Phys. Rev. Lett. **117**, 090402 (2016).
[62] A. I. Larkin and Y. N. Ovchinnikov, Sov. Phys. JETP **28**, 1200 (1969).
[63] S. H. Shenker and D. Stanford, J. High Energy Phys. 03 (2014) 067.
[64] S. H. Shenker and D. Stanford, J. High Energy Phys. 12 (2014) 046.
[65] S. H. Shenker and D. Stanford, J. High Energy Phys. 05 (2015) 132.
[66] D. A. Roberts and D. Stanford, Phys. Rev. Lett. **115**, 131603 (2015).
[67] D. Stanford, J. High Energy Phys. 10 (2016) 009.
[68] G. Styliaris, N. Anand, and P. Zanardi, Phys. Rev. Lett. **126**, 030601 (2021).
[69] X. Wang and P. Zanardi, Phys. Rev. A **66**, 044303 (2002).
[70] X. Wang, S. Ghose, B. C. Sanders, and B. Hu, Phys. Rev. E **70**, 016217 (2004).
[71] L. D'Alessio, Y. Kafri, A. Polkovnikov, and M. Rigol, Adv. Phys. **65**, 239 (2016).
[72] P. Hosur, X.-l. Qi, D. A. Roberts, and B. Yoshida, J. High Energy Phys. 02 (2016) 004.
[73] R. Fan, P. Zhang, H. Shen, and H. Zhai, Sci. Bull. **62**, 707 (2017).
[74] P. D. Bergamasco, G. G. Carlo, and A. M. F. Rivas, Phys. Rev. Research **1**, 033044 (2019).